COMPDYN 2011
III ECCOMAS Thematic Conference on
Computational Methods in Structural Dynamics and Earthquake Engineering
M. Papadrakakis, M. Fragiadakis, V. Plevris (eds.)
Corfu, Greece, 25–28 May 2011

A ROUGH COLLAPSE ASSESSMENT OF EARTHQUAKE EXCITED STRUCTURAL SYSTEMS VULNERABLE TO THE P-DELTA EFFECT

Christoph Adam[1], and Clemens Jäger[2]

[1] Department of Civil Engineering Sciences, University of Innsbruck
Technikerstr. 13, 6020 Innsbruck, Austria
e-mail: christoph.adam@uibk.ac.at

[2] Department of Civil Engineering Sciences, University of Innsbruck
Technikerstr. 13, 6020 Innsbruck, Austria
e-mail: clemens.jaeger@uibk.ac.at

Keywords: Collapse Capacity Spectrum, Equivalent Single-Degree-of-Freedom System, Global Collapse Capacity, Non-Deteriorating Inelastic Component Behavior, P-Delta Effect, Planar Multi-Story Frame Structure.

Abstract. *This paper addresses the prediction of the seismic collapse capacity of flexible non-deteriorating multi-story frame structures with regular layout, which are vulnerable to the de-stabilizing effect of gravity loads. The proposed time-saving and yet sufficient accurate methodologies are based on an equivalent single-degree-of-freedom system capable to cover the significant dynamic properties of the structure, and collapse capacity spectra. For a series of generic frame structures the global collapse capacity is assessed both with the proposed methodologies and the computationally expensive Incremental Dynamic Analysis procedure. From the outcomes of both methods it can be concluded that in the initial design process the proposed methodologies are an appropriate tool to assess sufficiently accurate the collapse capacity of P-delta sensitive regular moment resisting frame structures subjected to severe earthquake excitation.*

1 INTRODUCTION

Prediction of sidesway collapse of a structural building induced by severe earthquake excitation is the most prominent challenge in earthquake engineering [1]. Sidesway collapse may be the consequence of successive reduction of the lateral load bearing capacity due to strength and stiffness degradation. In very flexible buildings the destabilizing effect of gravity loads may lead to a negative post-yield stiffness, and thus, the structural collapse capacity is exhausted at a rapid rate when driven into its inelastic range of deformation even for stable hysteretic component behavior [2]. In many buildings the components are successively deteriorated until gravity takes over, and consequently the structure collapses. [1]

The focus of this paper is on the prediction of earthquake induced sidesway collapse of non-deteriorating flexible frame structures, which are vulnerable to the destabilizing effect of gravity loads, or, expressed in other words, vulnerable to the global P-delta effect. For a realistic *elastic* building the P-delta effect is usually negligible. However, it may become of significance for inelastic structural behavior when P-delta induces a negative post-yield slope of the lateral load-displacement relationship.

In earthquake engineering the global P-delta effect has been studied analytically, numerically, and experimentally in a series of papers. Representatively, the publications of Jennings and Husid [3], Bernal [4, 5], MacRae [6], Gupta and Krawinkler [7], Vian and Bruneau [8], and Lignos et al. [9] are cited. Asimakopoulos et al. [10], Villaverde [11], Ibarra and Krawinkler [12], Krawinkler et al. [1], and Haselton et al. [13] provide profound insights into the literature on studies dealing with dynamic collapse of earthquake excited structures. In comprehensive parameter studies, Adam and Jäger [14, 15, 16] treat rigorously the effects of P-delta on the collapse capacity of non-deteriorating SDOF systems, and the results are graphically displayed by means of collapse capacity spectra. In further studies, Adam and Jäger [2, 17] propose the collapse capacity spectrum methodology, based on an equivalent single-degree-of-freedom system and collapse capacity spectra, in an effort to determine the global collapse capacity of regular multi-story frame structures vulnerable to P-delta both time-efficient and yet accurate.

In the presented contribution the application of the original collapse capacity spectrum methodology as introduced in [2, 17] is described in detail. Additionally, a simplified collapse capacity spectrum methodology is recommended. The underlying concepts of equivalent single-degree-of-freedom (ESDOF) systems and collapse capacity spectra are reviewed. Both collapse capacity spectrum methods are evaluated for a series of generic frame structures, and the outcomes are set in contrast to “exact” collapse capacities of corresponding IDA studies.

2 GLOBAL COLLAPSE CAPACITY

2.1 Initial assessment of the structural vulnerability to global P-delta effects [2]

At first it must be assessed whether the considered structure is vulnerable to P-delta effects. Strong evidence delivers the result of a global pushover analysis [7]. During this nonlinear static analysis gravity loads are applied, and subsequently the structure is subjected to lateral forces. The magnitude of these forces with a predefined invariant load pattern is amplified incrementally in a displacement-controlled procedure. As a result the global pushover curve of the structure is obtained, where the base shear is plotted against a characteristic deformation parameter. In general the lateral displacement of the roof is selected as characteristic parameter. It is assumed that the shape of the global pushover curve reflects the global or the local mechanism involved when the structure approaches dynamic instability.

In Figure 1 the effect of gravity loads on the global pushover curve of a multi-story frame structure is illustrated. Figure 1(a) shows the global pushover curve, where gravity loads are either disregarded or of marginal importance. The pushover curve of Figure 1(b) corresponds to a very flexible multi-story frame structure with a strong impact of the P-delta effect leading to a reduction of the global lateral stiffness. In very flexible structures gravity loads even may generate a negative post-yield tangent stiffness as shown in Figure 1(b) [18]. If severe seismic excitation drives such a structure in its inelastic branch of deformation a state of dynamic instability may be approached, and the global collapse capacity is attained at a rapid rate. From these considerations follows that a gravity load induced negative post-yield tangent stiffness in the global pushover curve requires an advanced investigation of P-delta effects [7].

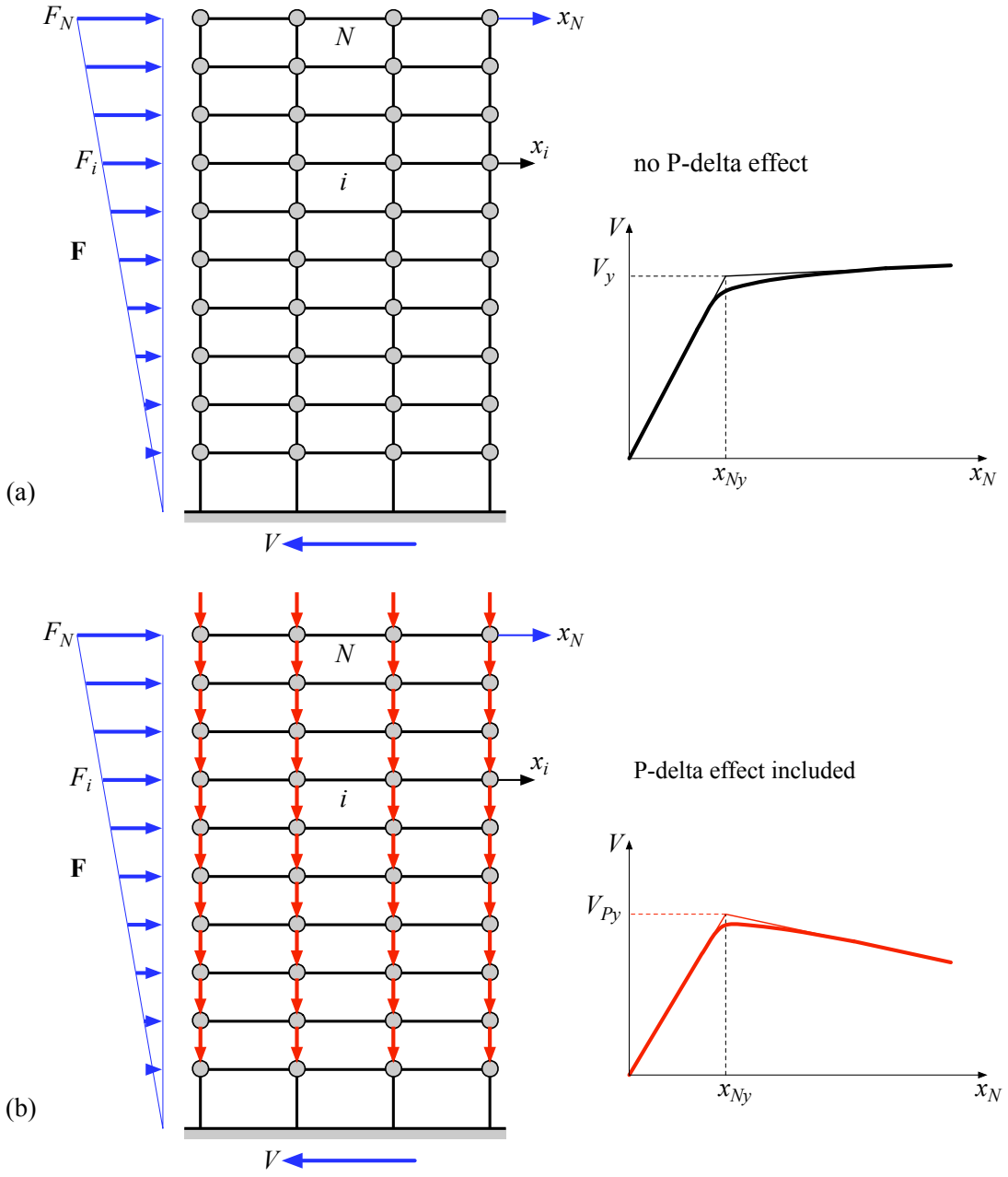

Figure 1: Multi-story frame structure and corresponding global pushover curves. (a) Pushover analysis disregarding P-delta. (b) Pushover analysis considering P-delta [2].

2.2 Assessment of the global collapse capacity

In the most general approach the Incremental Dynamic Analysis (IDA) procedure [19] is applied to determine the smallest earthquake intensity, which leads to structural collapse [2]. Thereby, for one acceleration time history of an earthquake record dynamic time history analyses are performed repeatedly, where in each subsequent run the intensity of the ground motion is incremented. As an outcome a characteristic seismic intensity measure is plotted against the corresponding maximum characteristic structural response quantity for each analysis. The procedure is stopped when the response grows to infinity, i.e. structural failure occurs. The corresponding intensity measure of the ground motion is referred to as collapse capacity of the building for this specific ground motion record. There is no unique definition of intensity of an earthquake record, however, the normalized 5% damped spectral acceleration at the structure's fundamental period $S_a(T_1)$ normalized by the product of the gravity of acceleration g and the base shear coefficient γ, $S_a(T_1) / (g\,\gamma)$, is widely accepted to characterize the intensity appropriately. γ is defined as ratio between yield base shear V_y (from the pushover curve without P-delta) and total weight W ($\gamma = V_y / W$).

Since the result of an IDA study strongly depends on the selected record, IDAs are performed for an entire set of n ground motion records, and the outcomes are evaluated statistically. In particular, the median of the sorted individual collapse capacities CC^i_{MDOF}, $i = 1,\ldots, n$, is considered as the representative collapse capacity for the examined structure and the regarded set of ground motion records,

$$CC_{MDOF} = med\left\langle CC^i_{MDOF}, i = 1,....,n \right\rangle \;, \quad CC^i_{MDOF} = \left.\frac{S_{a,i}}{g\gamma}\right|_{collapse} \tag{1}$$

Further significant statistical values of the collapse capacity are 16% and 84% percentiles of the individual outcomes, CC^{16}_{MDOF} and CC^{p84}_{MDOF}, respectively.

The IDA procedure requires the numerical solution of the equations of motions in each time step of each time history analysis, and as a consequence, is both time-consuming and computationally expensive. Thus, in [2, 17] for regular multi-story frame structures the so-called collapse capacity spectrum methodology has been proposed to obtain a quick but yet accurate approximation of the collapse capacity without performing time history analyses. The proposed methodology is based on the observation that the global P-delta effect is mainly governed by the fundamental mode. This holds also true if higher modes play a significant role in the dynamic structural response. Consequently, the collapse capacity is assessed utilizing an equivalent single-degree-of-freedom (ESDOF) system, and a collapse capacity spectrum [14, 15, 16]. This methodology is particular useful in engineering practice, because the structure can be evaluated with respect to its seismic collapse capacity in the initial design process.

3 FUNDAMENTALS OF THE COLLAPSE CAPACITY SPECTRUM METHODOLOGIES

3.1 Equivalent single-degree-of-freedom system

The ESDOF system is based on a time-independent shape vector $\boldsymbol{\phi}$, which describes the displacement vector $\mathbf{x}$ of the N-story MDOF frame structure regardless of its magnitude,

$$\mathbf{x} = \boldsymbol{\phi}\, x_N \;, \quad \phi_N = 1 \tag{2}$$

and on global pushover curves of the MDOF structure disregarding and considering gravity loads. In the corresponding pushover analyses the lateral load pattern must be selected to be affine to the displacement vector $\mathbf{x}$,

$$\mathbf{F} = \boldsymbol{\phi} F_N \tag{3}$$

and thus to the shape vector $\boldsymbol{\phi}$. x_N denotes the roof displacement, and F_N is the peak magnitude of the pushover load at the top of the frame structure, see Figure 1. The components ϕ_i of the shape vector $\boldsymbol{\phi}$ and the story masses $m_i, i = 1,...,N$, of the MDOF structure enter mass and participation factor of the ESDOF system. Transformation of bilinear idealizations of the global pushover curves, Figure 2(a), into the domain of the ESDOF system renders its backbone curves, Figure 2(b). However, consideration of the P-delta effect in the ESDOF system is not straight forward, because in contrast to a real SDOF system an ESDOF does not exhibit a unique stability coefficient. This behavior can be led back to the underlying global pushover curves with and without gravity loads. In a bilinear approximation of the pushover curves the stability coefficient θ_i in the post-yield range of deformation is larger than the elastic stability coefficient θ_e: $\theta_i > (>) \theta_e$ [18], compare with Figure 2(a). Thus, in [12, 2] it is proposed to assign an auxiliary backbone curve to the ESDOF system, which yields the backbone curve with applied gravity load by means of a single auxiliary stability coefficient θ_a [15]. Backbone curves of the ESDOF system are depicted in Figure 2(b): The blue bilinear curve represents the auxiliary backbone curve, and the corresponding red graph is the backbone curve with applied gravity load. For details of the ESDOF system it is referred to Fajfar [20], Adam et al. [21], and Ibarra and Krawinkler [12].

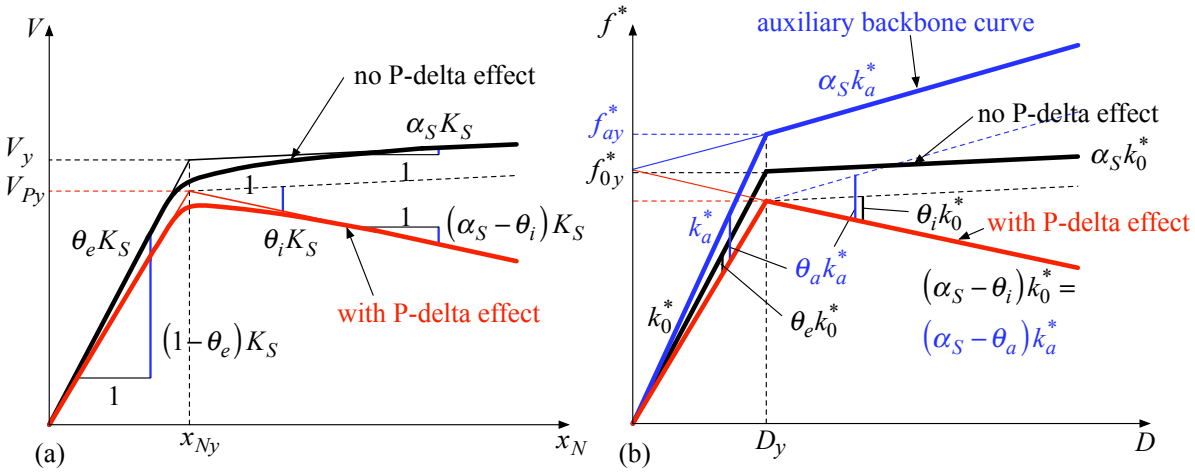

Figure 2: (a) Pushover curves with and without considering P-delta of a multi-story frame structure. (b) Backbone curves of the corresponding equivalent single-degree-of-freedom system.

The essential parameters of the ESDOF system required for the application of the collapse capacity spectrum methodology are the period T_a of the auxiliary ESDOF system, the auxiliary stability coefficient θ_a, and coefficient λ_{MDOF}. λ_{MDOF} transforms the collapse capacity from the SDOF domain into the domain of the MDOF system [2]. In [21, 12] these parameters are derived as:

$$T_a = 2\pi \sqrt{\frac{1-\alpha_S}{\upsilon}} \sqrt{\frac{x_{Ny}}{V_y}} \sqrt{\sum_{i=1}^{N} \phi_i m_i} \quad , \quad \theta_a = \frac{\theta_i - \theta_e \alpha_S}{\upsilon} \quad , \quad \upsilon = 1 - \theta_e + \theta_i - \alpha_S \qquad (4), (5), (6)$$

$$\lambda_{MDOF} = \frac{\left(\sum_{i=1}^{N} \phi_i m_i\right)^2}{\sum_{i=1}^{N} m_i \sum_{i=1}^{N} \phi_i^2 m_i} \tag{7}$$

Thereby, x_{Ny} denotes the roof displacement at onset of yield of the global pushover curve (without P-delta), see Figure 1.

If all story masses are equal, $m_i = m_s,\ i = 1,...,N$, than the expressions T_a and λ_{MDOF} reduce to

$$T_a = 2\pi\sqrt{\frac{1-\alpha_S}{\upsilon}}\sqrt{\frac{x_{Ny}}{V_y}}\sqrt{m_s\sum_{i=1}^{N}\phi_i} \quad , \quad \lambda_{MDOF} = \frac{\left(\sum_{i=1}^{N}\phi_i\right)^2}{N\sum_{i=1}^{N}\phi_i^2} \tag{8), (9}$$

For a linear shape vector with components $\phi_i = i/N,\ i = 1,...,N,$ and constant story height h, period T_a and coefficient λ_{MDOF} read as:

$$T_a = 2\pi\sqrt{\frac{1-\alpha_S}{\upsilon}}\sqrt{\frac{x_{Ny}m_s}{2V_y}}\sqrt{N+1} \quad , \quad \lambda_{MDOF} = \frac{3}{2}\frac{N+1}{2N+1} \tag{10), (11}$$

If the number of stories N is larger than 9, λ_{MDOF} can be approximated according to

$$\lambda_{MDOF} \underset{\forall N>9}{\approx} \frac{3}{4} \tag{12}$$

3.2 Collapse capacity spectrum

In [14, 15] it is shown that the record dependent collapse capacity of a real non-deteriorating SDOF system with bilinear backbone curve, which is vulnerable to the P-delta effect, is governed by the following quantities:

- Initial period of vibration T
- Viscous damping coefficient ζ
- Negative post-yield stiffness ratio $\theta - \alpha$
- Hysteretic loop

If the collapse capacity of a system with assigned hysteretic loop and fixed parameters ζ and $\theta - \alpha$ is plotted against the period of vibration, the resulting graph is referred to as collapse capacity spectrum for an individual ground motion record. Statistical evaluation of individual collapse capacity spectra, which belong to a specific set of earthquake records, leads to median, 16% and 84% percentile collapse capacity spectra. In [15] a rigorous study of the impact of the parameters specified above on collapse capacity spectra is presented.

In an effort to provide engineers a tool, which allows a quick estimation of the collapse capacity, in the same publication [15] design collapse spectra with a “smooth” shape have been derived via non-linear regression analyses. For a certain set of parameters an analytic relation

for base case median design collapse capacity spectra are defined. The impact of parameters, which differ from the base case, is considered by influence coefficients. For details see again [15]. Exemplarily, Figure 3 shows median design collapse capacity spectra (marked by circles) for a series of post-yield stiffness ratios $\theta-\alpha$, and the corresponding design collapse capacity spectra depicted by full lines. These collapse capacity spectra are based on the ATC63 far-field set of 44 ordinary ground motions [22], and have been derived for SDOF systems with bilinear hysteretic loops, and a viscous damping coefficient of $\zeta = 0.02$.

Application of design collapse capacity spectra is simple. An estimate of the elastic period of vibration *T*, damping coefficient ζ, stability coefficient θ, and hardening ratio α of the actual SDOF structure is to be determined. Subsequently, from the chart the corresponding collapse capacity *CC* can be read. Furthermore, in [15] analytic approximations of fragility curves based on a log-normal distribution of the collapse capacities are presented.

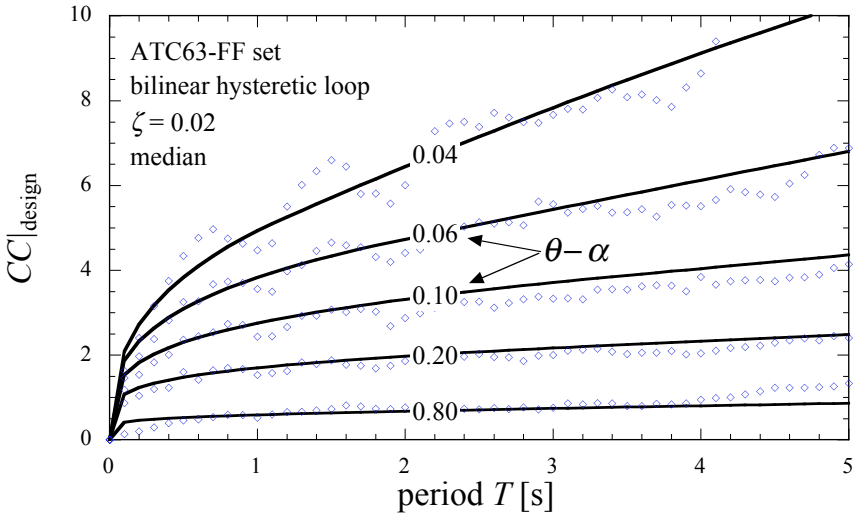

Figure 3: Median collapse capacity spectra (blue circles) and corresponding design collapse capacity spectra. Underlying parameters specified in the figure.

4 COLLAPSE CAPACITY SPECTRUM METHODOLOGIES

4.1 Original collapse capacity spectrum method

The procedure to derive an estimate of the collapse capacity of an MDOF frame structure based on the corresponding ESDOF system and collapse capacity spectra can be summarized as follows [2, 17]:

- Derive global pushover curves of the MDOF structure without and with gravity loads with an appropriate horizontal load pattern, e.g. according to the fundamental mode shape. If the post-yield stiffness of the gravity loaded structure is negative, determine the global collapse capacity as subsequently described.
- If feasible, perform a bilinear approximation of the pushover curves and identify the global hardening ratio α_S, and the elastic and inelastic stability coefficient θ_e and θ_i, respectively.
- Derive the auxiliary stability coefficient θ_a according Eq. (5), and derive the negative post-yield stiffness ratio $\theta_a - \alpha_S$.

- Select the shape vector ϕ affine to the horizontal load pattern of the pushover analyses, and derive the period T_a of the auxiliary ESDOF system according to Eqs (4), (8), or (10).
- Consult the appropriate design collapse capacity spectrum with respect to the underlying ground motion set, viscous damping ζ, hysteretic loop, and the negative post-yield stiffness $\theta_a - \alpha_S$, and read at the period T_a the median collapse capacity *CC*.
- Derive the coefficient λ_{MDOF} according Eq. (7), (9), or (11) and transform *CC* into the domain of the ESDOF system [2]:

$$CC_{ESDOF} = \frac{CC}{\lambda_{MDOF}} \tag{13}$$

  This outcome is an estimate of the actual median collapse capacity $CC_{MDOF} \approx CC_{ESDOF}$.
- If required, determine the 16% and 84% collapse capacities CC_{ESDOF}^{p16} and CC_{ESDOF}^{p84}, respectively, in analogy to the relations for a real SDOF system as derived by Adam and Jäger [15]:

$$CC_{ESDOF}^{p16} = CC_{ESDOF} / s_l^* \;, \quad s_l^*(T_a) = \frac{10}{7} T_a^{1/20} \tag{14, 15}$$

$$CC_{ESDOF}^{p84} = CC_{ESDOF} s_u^* \;, \quad s_u^*(T_a) = \frac{3}{2} T_a^{1/20} \tag{16, 17}$$

- Assuming that the uncertainties in the collapse capacities follow a log-normal distribution derive the fragility curve from [15]

$$\ln N(m, \sigma^2) \tag{18}$$

  with

$$m = \ln\left(CC_{ESDOF}\right) \;, \quad \sigma = \ln\sqrt{s_l^* s_u^*} \tag{19, 20}$$

4.2 Simplified collapse capacity spectrum method

In the following, a further simplification of the collapse capacity spectrum method for an even faster assessment of the global collapse capacity is suggested.

Inspection of Eqs (4), (8), and (10) reveals that only for large stability coefficients, i.e. $\theta_a - \alpha_S >> 0$, the P-delta effect has a severe impact on the auxiliary period T_a. However, for flexible systems the gradient of collapse capacity spectra is small, if $\theta_a - \alpha_S >> 0$, as it can be seen from Figure 3. Consequently, the collapse capacity *CC* is not much affected, if an approximation of the period enters the collapse capacity spectrum. Thus, it is proposed that a rough estimate of the fundamental structural period without taking account the gravity loads can be utilized instead of the auxiliary period T_a. This period replaces T_a in all relations of the original collapse capacity spectrum methodology.

A second simplification concerns the negative post-yield stiffness ratio. It can be shown that the auxiliary stability coefficient is always in-between the elastic and the inelastic stability coefficient. Hence, $\theta_i - \alpha_S$ is always larger than $\theta_a - \alpha_S$. Assuming that $\theta_i - \alpha_S$ is the characteristic post-yield stiffness ratio, the corresponding collapse capacity estimation is more

conservative compared to the value based on $\theta_a - \alpha_S$. For a fast and rough assessment of the collapse capacity the negative stiffness ratio derived according to $\theta_i - \alpha_S$ may be utilized.

Finally, for an initial collapse assessment a transformation coefficient of $\lambda_{MDOF} = 3/4$ may be employed, compare with Eq. (12).

5 EVALUATION OF THE COLLAPSE CAPACITY SPECTRUM METHODOLOGIES

For several generic multi-story frame structures as depicted in Figure 4(a) the original collapse capacity spectrum methodology and its simplified counterpart is evaluated setting its results in contrast with the "exact" collapse capacity based on IDAs. All stories of the single-bay structures of N stories are of uniform height h, and they are composed of rigid beams, elastic flexible columns, and rotational springs at the ends of the beams. Nonlinear behavior at the component level is modeled by non-degrading bilinear hysteretic behavior of the rotational springs (compare with Figure 4(b)) to represent the global cyclic response under seismic excitation. The strength of the springs is tuned such that yielding is initiated simultaneously at all spring locations in a static pushover analysis (without gravity loads) under an inverted triangular design load pattern. To each joint of the frames an identical point mass $m_i/2 = m_s/2$, $i = 1,...,N$, is assigned. The bending stiffness of the columns and the stiffness of the springs are tuned to render a straight line fundamental mode shape. Identical gravity loads are assigned to each story to simulate P-delta effects. This implies that axial column forces due to gravity increase linearly from the top to the bottom of each frame. The frame structures have a fundamental period of vibration of $T_1 = 0.2\,N$, which makes them rather flexible.

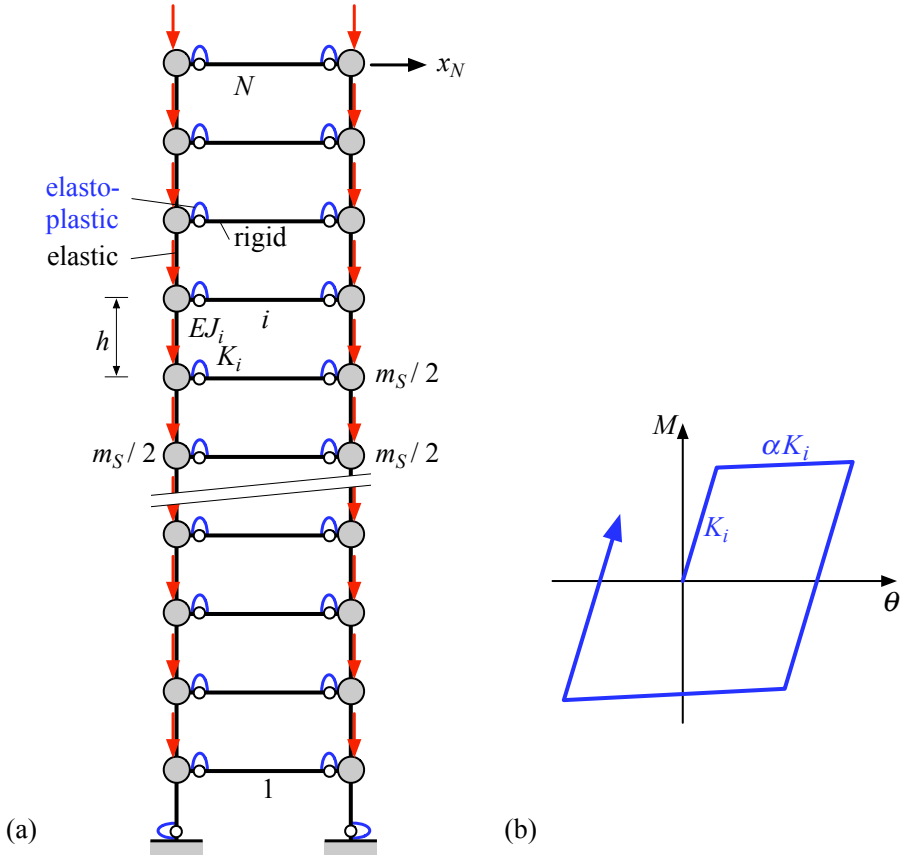

Figure 4: (a) Planar generic multi-story frame structure. (b) Bilinear hysteretic loop of the rotational springs.

In a first example problem an 18-story frame structure is considered. The fundamental period is $T_1 = 3.6$ s. The hardening coefficient of all rotational springs is chosen to be $\alpha = 0.01$, the ratio of dead load plus life load to dead load is $\vartheta = 1.0$. Structural damping is considered by means of mass and stiffness proportional Rayleigh damping of 2% of the first mode and 2% of that mode, where the sum of modal masses exceeds 95% of the total mass.

In Figure 5 the outcomes of an IDA procedure utilizing the 44 records of the ATC63-FF set are shown. Each IDA curve displayed with light gray lines belongs to a specific record. Thereby, the non-dimensional excitation intensity $S_a / (g\gamma)$ is plotted against the normalized roof displacement x_N / S_d. S_a and S_d are the spectral acceleration and spectral displacement, respectively, at the period $T = T_1$ of the 5% damped response spectrum of the considered record. The lowest intensity, where a specific IDA curve exhibits a horizontal tangent, is the collapse capacity of the MDOF structure for the corresponding earthquake record. This figure reveals the large record dependent dispersion of the individual collapse capacities. A blue fat line represents the median IDA curve. From the results the "exact" median collapse capacity of $CC_{MDOF} = 3.33$ can be identified. Additionally, fat black lines correspond to the 16% percentile and 84% percentile IDA curves. The 16% percentile and 84% percentile collapse capacities are $CC^{16}_{MDOF} = 2.33$ and $CC^{84}_{MDOF} = 5.45$, respectively.

The assessment of the collapse capacity according to the collapse capacity spectrum methodology requires the identification of the elastic and the inelastic stability coefficient, and the global hardening ratio from global pushover curves without and with P-delta effect. The pushover curves of the structure are depicted in Figure 6. The parameters are determined as: $\theta_e = 0.073$, $\theta_i = 0.222$, $\alpha_S = 0.013$. Subsequent evaluation of Eqs (5) and (10) yields the auxiliary stability coefficient and the auxiliary period, respectively: $\theta_a = 0.195$, $T_a = 3.35$ s. The transformation coefficient λ_{MDOF}, Eq. (11), is derived as 0.770. The required post-yield stiffness ratios are: $\theta_a - \alpha_S = 0.182$, $\theta_i - \alpha_S = 0.209$.

Figure 7 shows the utilized 2% damped median design collapse capacity spectra for bilinear hysteretic behavior and the ATC63-FF record set [15]. Herein, it is illustrated, how the median collapse capacities for the proposed methodologies are determined.

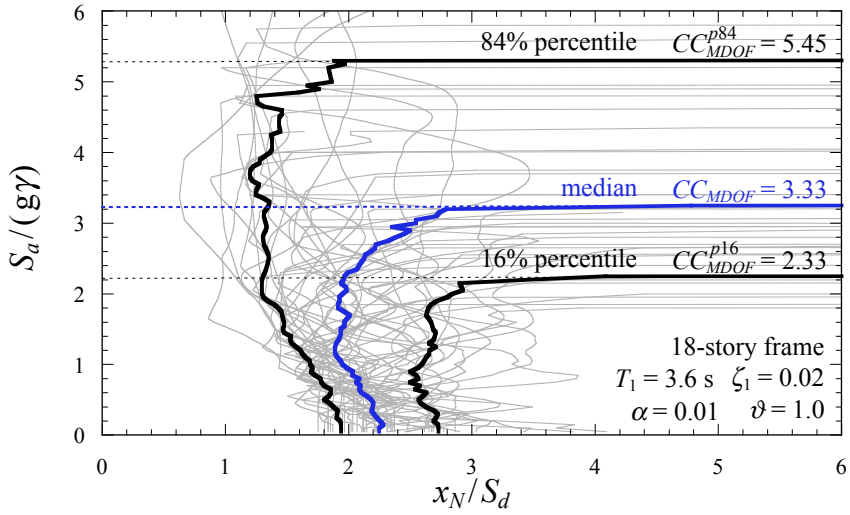

Figure 5: IDA curves for 44 ground motions of the ATC63-FF set. Median, 16% percentile, and 84% percentile IDA curves. Generic 18-story frame structure with a fundamental period of vibration of 3.6 s.

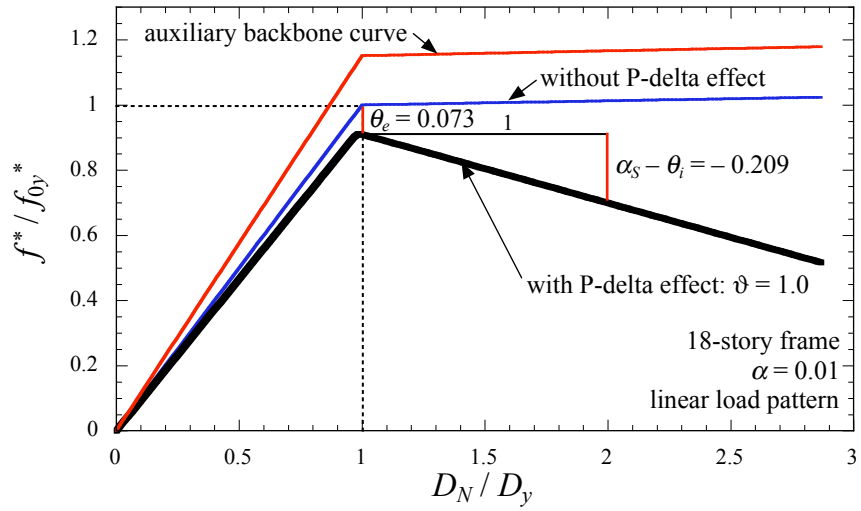

Figure 6: Backbone curves of the equivalent single-degree-of-freedom system for a generic 18-story frame structure.

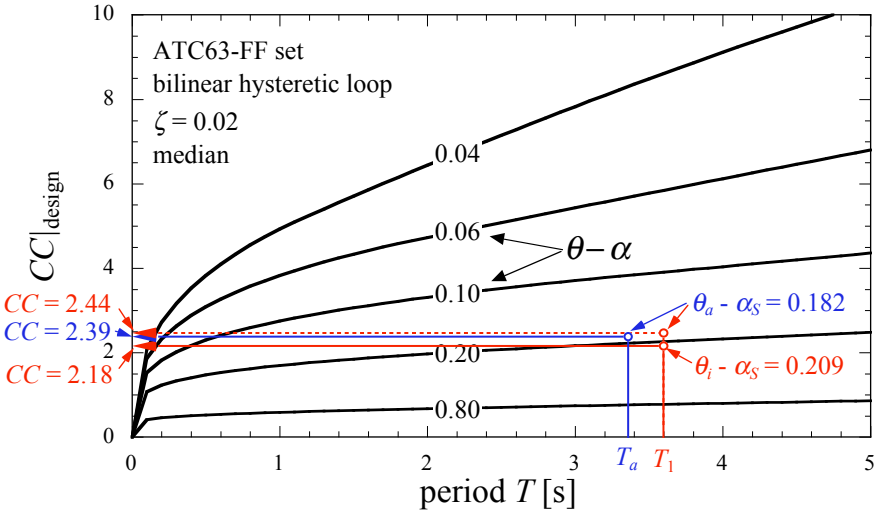

Figure 7: Median design collapse capacity spectra applied for prediction of the median collapse capacity of a generic 18-story frame structure. Different collapse capacity spectrum methodologies.

In Table 1 the outcomes of different collapse capacity assessment methodologies are specified. The collapse capacity of the second column corresponds to the "exact" outcome of an IDA study based on the 44 earthquake records of the ATC63-FF set, whereas the results of columns three, four and five are based on ESDOF systems and collapse capacity spectra. Furthermore, in this table the underlying parameters of the different collapse capacity spectrum approximations are listed.

Inspection reveals that the median collapse capacity of the third column, $CC_{ESDOF} = 3.10$, determined by the original collapse capacity methodology, is about 93% of the "exact" counterpart, and thus a conservative estimate. The simplified collapse capacity spectrum methodology yields a median collapse capacity $CC_{ESDOF} = 2.91$, compare with column five. An "intermediate" simplified capacity spectrum methodology, where the negative post-yield stiffness of the auxiliary ESDOF $\theta_a - \alpha_S$, and the fundamental period T_1 of the frame structure enters the collapse capacity spectrum leads to $CC_{ESDOF} = 3.16$, which is the approxima-

tion closest to the "exact" outcome. The difference between the "exact" and approximated percentile collapse capacities is of the same order as for the median values, compare with Table 1.

Figure 8 shows the counted collapse fragility curve from the IDA study, and several approximated "smooth" fragility curves of the considered 18-story frame structure. The blue line is a "best fit" of the counted fragilities employing the maximum likelihood method. The black and red lines are based on log-normal approximations taking into account different values of the percentiles. The fragility curves according to the collapse capacity spectrum methodologies (displayed in red color) are derived employing Eqs (14) to (20). The curve displayed in black color has been derived using counted median, 16% and 84% percentiles from the IDA study.

Subsequently, the median collapse capacity of 12 generic multi-story frame structures vulnerable to P-delta is evaluated. The number of stories N ranges from 15 to 24. Spring hardening ratios α of 1%, 2%, and 3% are employed, and viscous damping ζ_1 of the fundamental mode of 2% and 5% is taken into account. The considered dead load plus life load to dead load ratios ϑ are 1.0, 1.2, and 1.4. In Table 2 the properties of the individual frames are specified.

Methodology	IDA study	Original collapse capacity spectrum methodology	Simplified collapse capacity spectrum methodology	Simplified collapse capacity spectrum methodology
Period		$T_a = 3.35$ s	$T_1 = 3.60$ s	$T_1 = 3.60$ s
Post-yield stiffness ratio		$\theta_a - \alpha_S = 0.182$	$\theta_a - \alpha_S = 0.182$	$\theta_i - \alpha_S = 0.209$
Transformation coefficient		$\lambda_{MDOF} = 0.770$	$\lambda_{MDOF} = 0.770$	$\lambda_{MDOF} = 3/4$
CC from spectrum		2.39	2.44	2.18
Median collapse capacity	$CC_{MDOF} = 3.33$	$CC_{ESDOF} = 3.10$	$CC_{ESDOF} = 3.16$	$CC_{ESDOF} = 2.91$
16% percentile collapse capacity	$CC^{16}_{MDOF} = 2.33$	$CC^{16}_{ESDOF} = 2.04$	$CC^{16}_{ESDOF} = 2.07$	$CC^{16}_{ESDOF} = 1.91$
84% percentile collapse capacity	$CC^{84}_{MDOF} = 5.45$	$CC^{84}_{ESDOF} = 4.94$	$CC^{84}_{ESDOF} = 5.05$	$CC^{84}_{ESDOF} = 4.65$
CC_{ESDOF} / CC_{MDOF}	1	0.93	0.95	0.87
$CC^{p16}_{ESDOF} / CC^{p16}_{MDOF}$	1	0.88	0.89	0.82
$CC^{p84}_{ESDOF} / CC^{p84}_{MDOF}$	1	0.91	0.93	0.85

Table 1: Median, 16% percentile, and 84% percentile collapse capacity of a generic 18-story frame structure. "Exact" outcome of an IDA study, and results from collapse capacity spectrum methodologies based on equivalent single-degree-of-freedom systems.

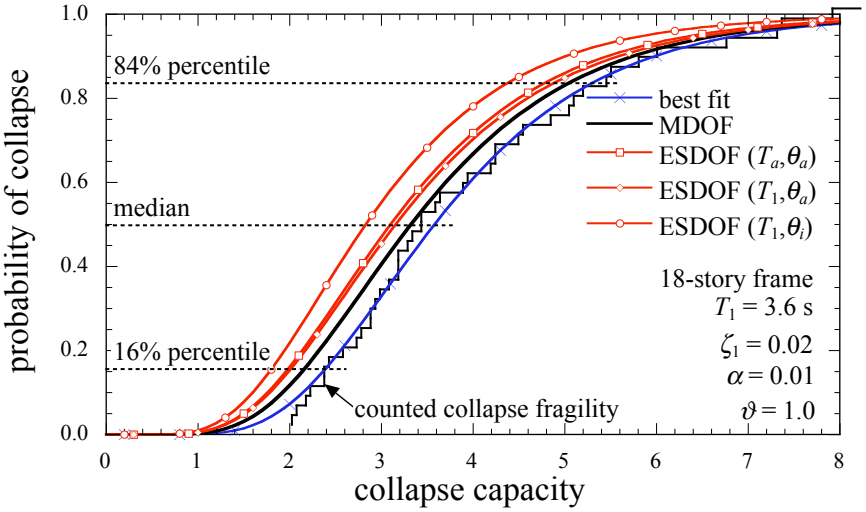

Figure 8: Counted fragility curve and "smooth" approximations based on log-normal distribution of an generic 18-story frame structure.

Frame ID	Number of stories N	Fundamental period T_1 [s]	Spring hardening ratio α	Damping ratio ζ_1	Gravity load ratio ϑ
1	18	3.6	0.03	0.05	1.0
2	18	3.6	0.03	0.05	1.2
3	18	3.6	0.03	0.05	1.4
4	15	3.0	0.03	0.05	1.0
5	21	4.2	0.03	0.05	1.0
6	24	4.8	0.03	0.05	1.0
7	18	3.6	0.02	0.05	1.0
8	18	3.6	0.01	0.05	1.0
9	18	3.6	0.03	0.02	1.0
10	18	3.6	0.03	0.02	1.2
11	18	3.6	0.01	0.02	1.0
12	18	3.6	0.02	0.02	1.2

Table 2: ID and properties of the considered generic multi-story frame structures.

Figure 9 shows for each frame the median collapse capacity from an IDA study of the actual multi-story structure (black bar), and from application of the collapse capacity spectrum methodologies (colored bars). The outcomes of the original collapse capacity spectrum methodology, based on the auxiliary structural period T_a and the auxiliary stability coefficient θ_a, are depicted in red. The blue bar corresponds to results from the simplified collapse capacity spectrum methodology utilizing the fundamental structural period T_1 and the inelastic stability coefficient θ_i. The collapse capacities depicted in green are derived from an "intermedi-

ate" simplified collapse capacity spectrum methodology, where T_1 and θ_a enter the analysis. It is readily observed that the 15-story frame (frame ID 4) exhibits the largest global collapse capacity. The median collapse capacity of structures with ID 3, 6, and 12 is of the same magnitude. Comparison reveals that for all considered structures the "exact" IDA results are of the same magnitude as their counterparts of the collapse capacity spectrum methodologies.

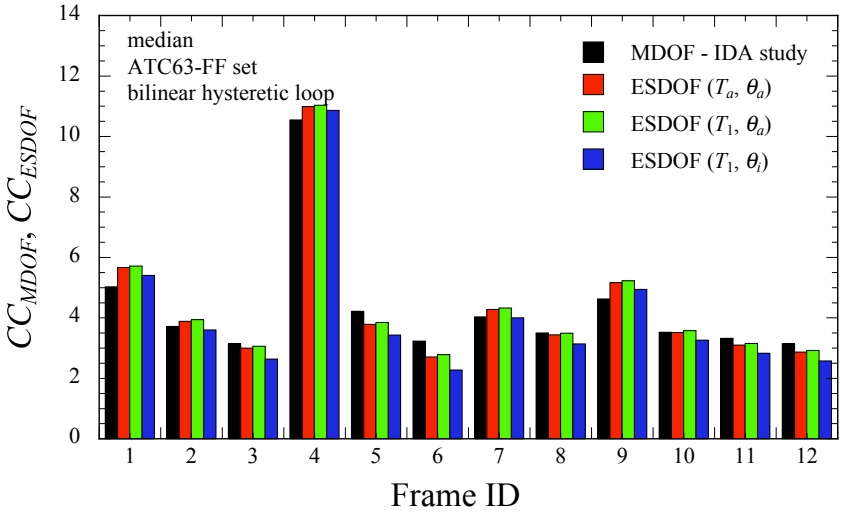

Figure 9: Global collapse capacities for a series of generic multi-story frame structures according to Table 2. "Exact" outcome from IDA studies, and results from collapse capacity spectrum methodologies based on equivalent single-degree-of-freedom systems.

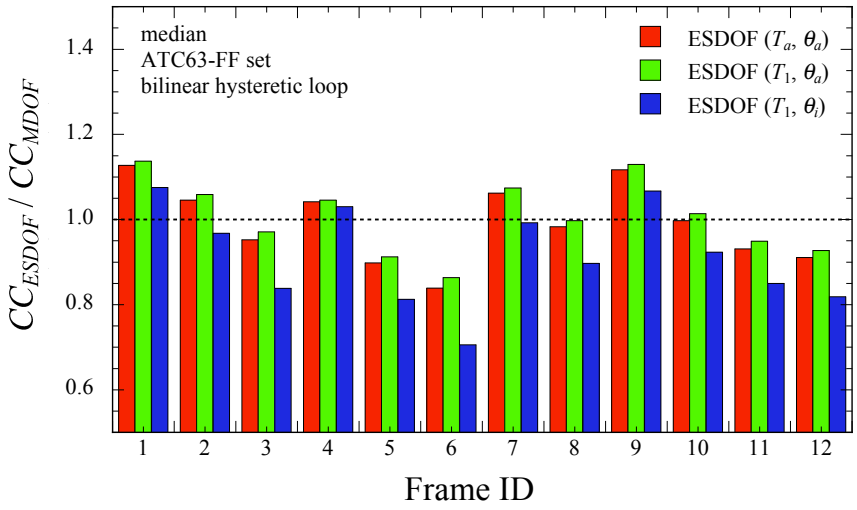

Figure 10: Global collapse capacity ratios for a series of generic multi-story frame structures according to Table 2. Results from collapse capacity spectrum methodologies based on equivalent single-degree-of-freedom systems related to the "exact" outcome from IDA studies.

The difference in percent of the individual results for each frame is illustrated in Figure 10, where the ratios of collapse capacities from ESDOF considerations to the "exact" outcomes are shown. A ratio of one implies that both considered methods predict the same collapse capacity. If the ratio is smaller than one, the collapse capacity is underestimated by the collapse capacity spectrum methodology, i.e. the outcome is conservative compared to the "exact" value. It can be seen that for frames 1, 2, 4, 7, and 9 the collapse capacity spectrum method-

ologies lead to slightly non-conservative predictions up to 12%. For frames 5 and 6 predictions are very conservative.

Setting in contrast the results of the individual collapse capacity spectrum methodologies for each frame separately reveals that the simplified method renders the smallest collapse capacity, and thus, for some structures over-conservative predictions.

However, taking into account the underlying simplifications it can be concluded that all applied collapse capacity spectrum methodologies are capable to yield a collapse capacity estimate, which is sufficiently accurate for the initial design process of buildings.

6 CONCLUSIONS

The seismic collapse capacity of a series of non-deteriorating multi-story frame structures vulnerable to the destabilizing effect of gravity loads was assessed employing the collapse capacity spectrum methodology, a simplified subspecies of this methodology, and the IDA procedure. Evaluation of the results reveals that both the original and simplified capacity spectrum methodology render sufficient accurate estimates of the global collapse capacity, and thus can be utilized efficiently in the initial design process of buildings.

REFERENCES

[1] H. Krawinkler, F. Zareian, D.G. Lignos, L.F. Ibarra, Prediction of collapse of structures under earthquake excitations. M. Papadrakakis, N.D. Lagaros, M. Fragiadakis eds. *2nd International Conference on Computational Methods in Structural Dynamics and Earthquake Engineering (COMPDYN 2009)*, Rhodes, Greece, June 22-24, 2009, CD-ROM paper, paper no. CD449, 2009.

[2] C. Adam, C. Jäger, Seismic induced global collapse of non-deteriorating frame structures. Papadrakakis, M., Fragiadakis, M., Lagaros, N.D., eds. *Computational Methods in Earthquake Engineering*, pp. 21 - 40, Springer, 2011.

[3] P.C. Jennings, R. Husid, Collapse of yielding structures during earthquakes. *Journal of the Engineering Mechanics Division, Proc. ASCE* **94**, 1045-1065, 1968.

[4] D. Bernal, Amplification factors for inelastic dynamic P-Δ effects in earthquake analysis. *Earthquake Engineering and Structural Dynamics* **15**, 635-651, 1987.

[5] D. Bernal, Instability of buildings during seismic response. *Engineering Structures* **20**, 496-502, 1998.

[6] G.A. MacRae, P-Δ effects on single-degree-of-freedom structures in earthquakes. *Earthquake Spectra* **10**, 539-568, 1994.

[7] A. Gupta, H. Krawinkler, *Seismic demands for performance evaluation of steel moment resisting frame structures*. Report No. 132. The John A. Blume Earthquake Engineering Research Center, Department of Civil and Environmental Engineering, Stanford University, Stanford, CA, 1999.

[8] D. Vian, M. Bruneau, Tests to structural collapse of single degree of freedom frames subjected to earthquake excitation. *Journal of Structural Engineering* **129**, 1676-1685, 2003.

[9] D.G. Lignos, H. Krawinkler, A. Whittaker, Prediction and validation of sidesway collapse of two scale models of a 4-story steel moment frame. *Earthquake Engineering and Structural Dynamics*, accepted for publication.

[10] A.V. Asmialopoulos, D.L. Karabalis, D.E. Beskos, Inclusion of P- Δ effect in displacement-based seismic design of steel moment resisting frames. *Earthquake Engineering and Structural Dynamics* **36**, 2171-2188, 2007.

[11] R. Villaverde, Methods to assess the seismic collapse capacity of building structures: State of the art. *Journal of Structural Engineering* **133**, 57-66, 2007.

[12] L.F. Ibarra, H. Krawinkler, *Global collapse of frame structures under seismic excitations*. Report No. PEER 2005/06, Pacific Earthquake Engineering Research Center, University of California, Berkeley, CA, 2005.

[13] C.B. Haselton, A.B. Liel, G.G. Deierlein, Simulating structural collapse due to earthquakes: Model idealization, model calibration, and numerical simulation algorithms. Papadrakakis M., Lagaros, N.D., Fragiadakis, M., eds. *2nd International Conference on Computational Methods in Structural Dynamics and Earthquake Engineering* (*COMPDYN 2009*), June 22-24, 2009, Rhodes, Greece, CD-ROM paper, paper no. CD497, 2009.

[14] C. Adam, P-delta effects in earthquake excited structures. Yamanaka, H., Morikawa, H., Satoshi, Y. eds. Proc. *Sixth International Conference on Urban Earthquake Engineering*, Tokyo Institute of Technology, Japan, March 3-4, 2009, pp. 231 – 234, 2009.

[15] C. Adam, C. Jäger, Seismic collapse capacity of basic inelastic structures vulnerable to the P-delta effect. *Earthquake Engineering and Structural Dynamics* (submitted for publication).

[16] C. Adam, C. Jäger, Collapse capacity spectra for finite ductility thresholds, to be published.

[17] C. Adam, C. Jäger, Assessment of the dynamic stability of tall buildings subjected to severe earthquake excitation. *Highrise Towers and Tall Buildings 2010*, International Conference at the Technische Universität München, Germany, April 14 - 16, 2010, CD-ROM paper, 8 pp., 2010.

[18] R.A. Medina, H. Krawinkler, *Seismic demands for nondeteriorating frame structures and their dependence on ground motions*. Report No. 144. The John A. Blume Earthquake Engineering Research Center, Department of Civil and Environmental Engineering, Stanford University, Stanford, CA, 2003.

[19] D. Vamvatsikos, C.A. Cornell, Incremental dynamic analysis. *Earthquake Engineering and Structural Dynamics* **31**, 491-514, 2002.

[20] P. Fajfar, Structural analysis in earthquake engineering - a breakthrough of simplified non-linear methods. *12th European Conference on Earthquake Engineering*, CD-ROM paper, Paper Ref. 843, 20 pp., Elsevier, 2002.

[21] C. Adam, L.F. Ibarra, H. Krawinkler, Evaluation of P-delta effects in non-deteriorating MDOF structures from equivalent SDOF systems. *13th World Conference on Earthquake Engineering*, August 1 - 6, 2004, Vancouver B.C., Canada. DVD-ROM paper, 15 pp., Canadian Association for Earthquake Engineering, 2004.

[22] FEMA P695 - Quantification of Building Seismic Performance Factors. Federal Emergency Management Agency, Washington D.C., 2009.